

DESIGN OF A WING SHAPE FOR STUDY OF HYPERSONIC CROSSFLOW TRANSITION IN FLIGHT

A. GODIL† and A. BERTELROD‡

†HTC/NASA Langley Research Center, Hampton, VA 23665, U.S.A.

‡AS&M/NASA Langley Research Center, Hampton, VA 23665, U.S.A.

Abstract—Computational fluid dynamics methods were used in the design of a wing shape for study of hypersonic crossflow transition in flight. The flight experiment is to be performed on the delta wing of the first stage of a Pegasus launch vehicle as a piggy-back experiment to support boundary-layer stability code development and validation. The design goal is to obtain crossflow-induced transition at 20–40% of the chord for a flight Mach number of approximately six. The present paper describes the design and analysis process utilized to obtain desired glove shape. A variety of schemes were used in the design, ranging from simple empirical crossflow correlations to three-dimensional Navier–Stokes codes in conjunction with linear stability/ N -factor computations. The sensitivity to various parameters, such as trajectory variations, allowable wing thickness, leading-edge radius and surface temperature, is also discussed.

NOMENCLATURE

C_0	chord length measured normal to leading edge
$L_{0.01W_{max}}$	crossflow length scale
M_c	edge Mach number
N	N -factor
p	pressure
Re_{cf}	crossflow Reynolds number
Re_{t-cf}	crossflow transition Reynolds number
\bar{R}^*	attachment-line similarity parameter
s	contour tangent to the group velocity
T	temperature
T_{wall}	wall temperature
$T_{adiabatic}$	adiabatic wall temperature
U_{10}	non-dimensional chordwise velocity gradient at the attachment line
U_c	velocity at the edge of the boundary layer
U_∞	free-stream velocity
U, V, W	total velocity components in the chordwise, normal and spanwise direction
$\bar{U}, \bar{V}, \bar{W}$	mean-flow velocity components
$\bar{u}, \bar{v}, \bar{w}$	disturbance velocity components
x, y, z	chordwise, normal and spanwise Cartesian coordinates
α	streamwise wavenumber
β	spanwise wavenumber
γ	specific heat ratio
δ	boundary layer thickness
λ	wavelength
ν	kinematic viscosity
ρ	density
σ	spatial growth rate
ψ	wave angle
ω	frequency
ω_t	temporal growth rate

INTRODUCTION

Renewed interest in airbreathing flight at hypersonic speeds [e.g. the National Aero-Space Plane (NASP)] has prompted research in transition for high speed flow. The area of transition from laminar to turbulent flow is of both fundamental and practical importance, since the onset of transition not only increases the viscous drag but also the surface heating and

dictates the forebody boundary-layer thickness entering the inlet of NASP-class vehicles.

A flight experiment is in preparation to characterize crossflow transition under hypersonic Mach numbers and conditions of interest for the development of NASP. While linear stability codes (such as COSAL¹) are becoming common tools for transition estimation through supersonic speeds, the experimental verification required for assessment of the code reliability for prediction of crossflow transition is lacking at hypersonic speeds. It is therefore imperative that these stability codes be validated for transition estimation at hypersonic speeds through carefully planned and executed experiments. The current experiment is to be performed in flight rather than in a wind tunnel to avoid the effects of sound radiation from the turbulent, nozzle-wall boundary layers and of facility-dependent free-stream turbulence fields. It will be performed on the delta wing of stage 1 of the Pegasus launch vehicle in a Mach number range of 5–8 and at altitudes ranging from 35 to 70 km. To limit the changes to the launch vehicle, it was decided to conduct the experiment utilizing the original wing. A part-span glove was mounted in the forward mid-span region and faired onto this wing.

The wing-glove shape was designed by utilizing a Navier–Stokes code in conjunction with a linear stability code. The aim of the glove design was to obtain the crossflow-dominated transition on the gloved portion of the wing, at 20–40% of the chord at flight Mach 6. The glove shape was designed with the following objectives: (1) flow at the attachment line must be laminar; (2) the crossflow instability can be maximized by increasing the pressure gradient along the chord; (3) second mode and Tollmien–Schlichting (TS) instability can be attenuated by having a favorable streamwise pressure gradient over the entire glove.

PEGASUS

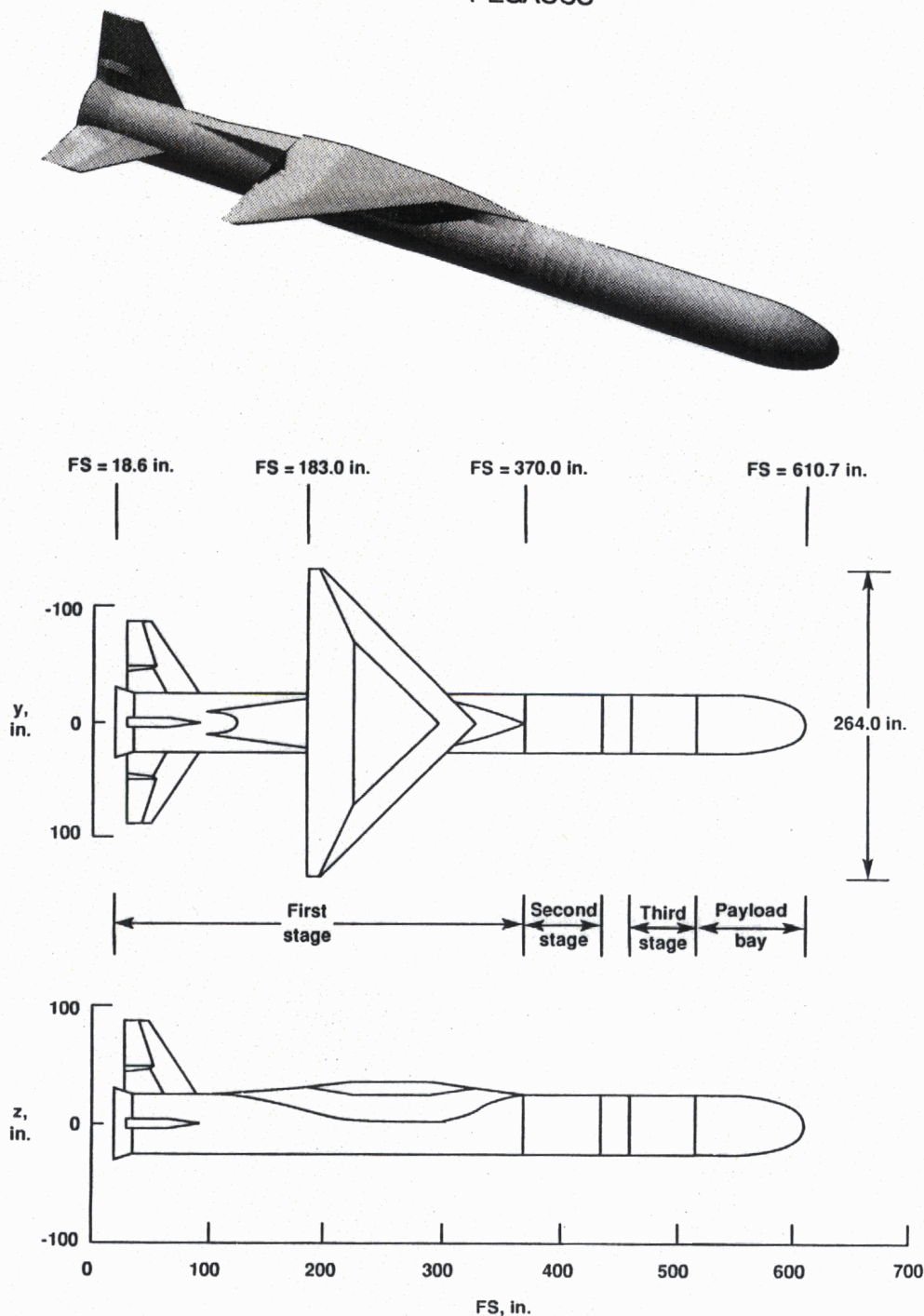


Fig. 1. Geometry of Pegasus launch vehicle.

The present paper describes the design and analysis process utilized to obtain the desired glove shape for flight studies of crossflow transition. The sensitivities to various parameters, such as trajectory variations, allowable wing thickness, leading-edge radius and surface temperature, are also discussed. Computational codes of varying complexity have been used in the design, ranging from conical boundary-layer

and stability codes to full three-dimensional Navier-Stokes solvers. A central issue in the present work was developing the capability to perform stability computations utilizing the fully three-dimensional hypersonic mean flow solutions from the Navier-Stokes code. In the past, most stability computations were restricted to two-dimensional and simplified three-dimensional flows (e.g. infinite swept

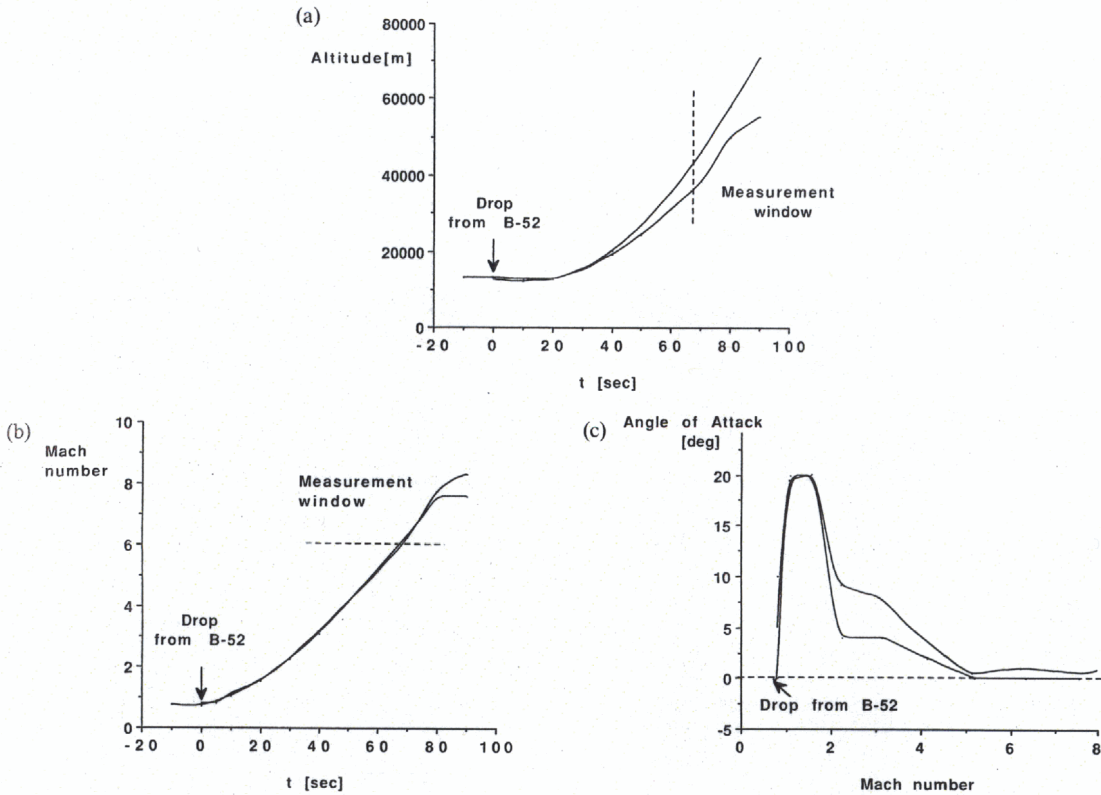


Fig. 2. Typical trajectories of the Pegasus flight. (a) altitude vs time; (b) Mach number vs time; (c) angle of attack vs Mach number.

wings), where the mean flow was usually obtained by boundary-layer codes. Exceptions are the recent stability work of Spall and Malik² and Iyer and Spall.³

GEOMETRY AND TRAJECTORY

The geometry of the baseline Pegasus flight vehicle is shown in Fig. 1. The vehicle consists of a blunt-nosed cylindrical body 1.22 m (4 ft) in diameter and

15.24 m (50 ft) in length, with a delta wing mounted on top. An account of the vehicle itself, its design and the results from the first flight can be found in Refs 4 and 5. Because both local Reynolds number and temperature history influence the transition location, the design of the glove shape for the transition experiment is very much dependent on the trajectory. Figure 2a-c shows the ranges of altitude, Mach number and angle-of-attack for typical trajectories

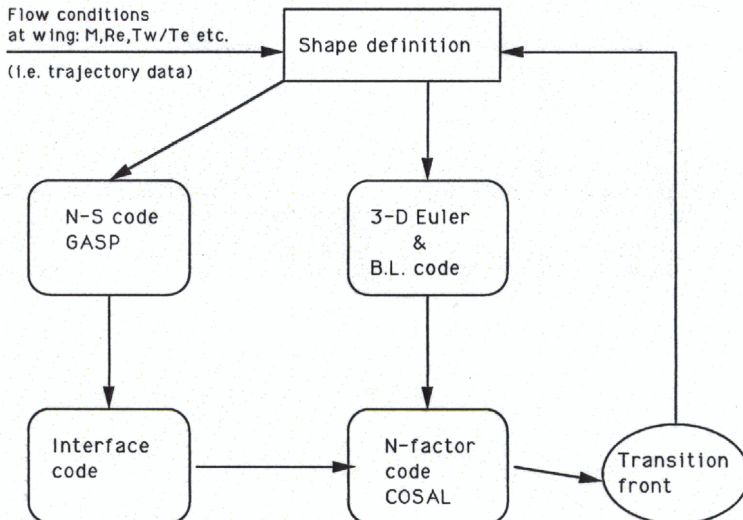


Fig. 3. Computational methods employed.

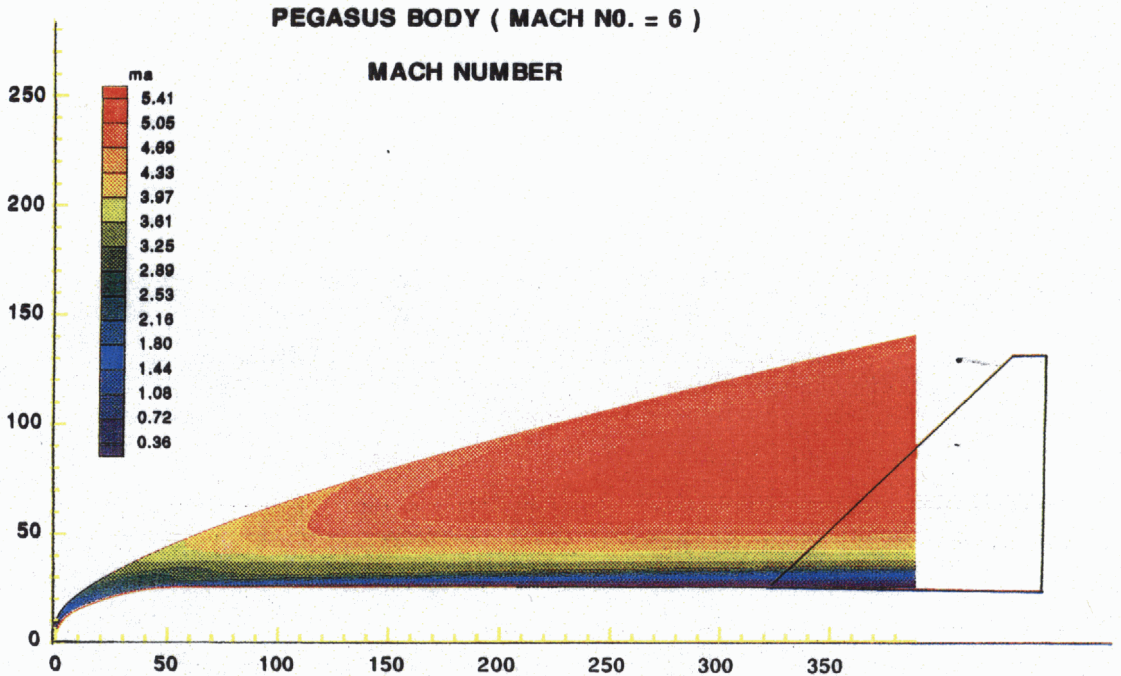


Fig. 4. Mach number contours and position of the bow shock for the blunt nosed body of Pegasus.

considered. Data obtained above Mach 5 are of prime interest and the requirements specified for the transition experiment include an angle of attack of zero or as close to zero as possible. As can be seen in Fig. 2c, this requirement is met roughly at Mach 5 and beyond, after the high angle-of-attack values used to gain altitude during the initial post-launch flight.

COMPUTATIONAL STRATEGY

The computational strategy utilized for the wing-glove design employed several levels of computational and geometrical complexity (see Fig. 3). Obtaining the overall flow field solution involved computation of the axisymmetric flow field about the vehicle forebody without the wings present, followed by calculation of the flow over wings with either the baseline wing-profile shape or the glove profile extending across the wing. Initially, simple codes, such as wing-only Euler codes, a three-dimensional boundary-layer code and the COSAL stability code, were used for different glove shapes to initially survey the parameter field, looking at transition location dependence on Mach and Reynolds number variations, as well as surface temperature effects. The Navier-Stokes code and the stability code were then used to obtain additional information at selected conditions and verify the transition results obtained using the simpler methods and geometries. Finally, the Navier-Stokes computations of the full vehicle were performed to determine the location of the shocks generated at various junctions. Each of these stages are described in detail below.

Bow shock

Axisymmetric viscous shock-layer calculations for the Pegasus cylindrical body with a blunt nose were performed for Mach 6 and pressure of 557 N m^{-2} . The code solves the time-dependent viscous shock-layer equations in body-oriented coordinates with shock fitting using a MacCormack scheme.⁶ The computational results for Mach 6, shown in Fig. 4, indicate that the bow shock does not impinge on the wing. Since the Pegasus delta wing is located off the fuselage axis, the wing will be exposed to spatial gradients of angle of attack and sideslip. At the glove location the angle of attack and sideslip range from 0.5 to 1.5° . The Mach number also varies considerably, as shown in Fig. 4, but for simplified calculations a representative

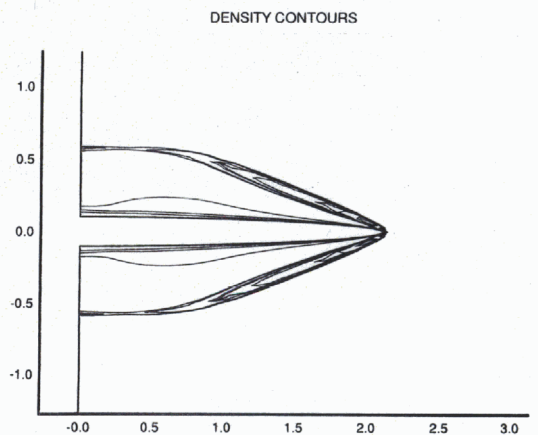


Fig. 5. Computed shock wrapping around the delta wing at Mach 6.

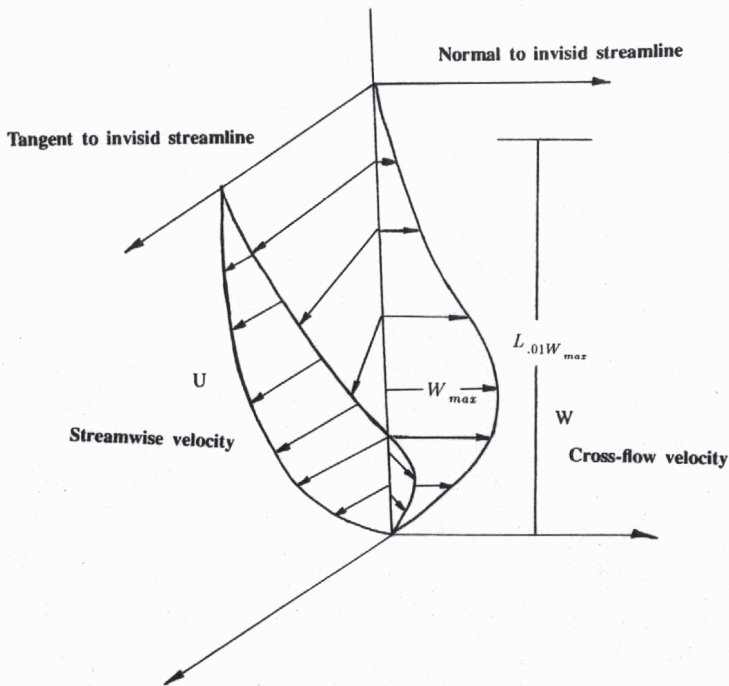


Fig. 6. Definition of streamwise and crossflow velocity profiles.

uniform inflow Mach number at zero angle of attack was used.

Mean-flow calculations of the delta wing

The Navier–Stokes calculations were performed on the delta wing in the absence of the fuselage. The GASP code⁷ was used in the calculations and is described in a later section. The three-dimensional grid was generated in planes at constant streamwise location.⁸ The grid points were clustered near the surface with at least 30 points in the boundary layer; the total number of grid points used was close to 3.5×10^5 . At the inflow boundary, a representative constant Mach number of 5.4 and zero angle of attack were selected as representative of flow from the bow shock calculation at Mach 6. A sensitivity analysis was performed for a 1° angle of attack; only a small influence could be noted. Figure 5 shows the computed shock wrapped around the leading edge of the 45° delta wing.

The surface temperature is expected to vary both with location on the body and with time along the trajectory and computations were therefore performed for both adiabatic-wall and cold-wall ($T_{wall}/T_{adiabatic} = 0.4$) conditions. For the cold-wall case, the wall temperature was obtained by multiplying the wall temperature from the adiabatic wall calculations by a factor of 0.4.

LINEAR STABILITY

Compressible linear stability theory was used for estimation of transition onset location via the conventional e^N method. The value of N -factor

for transition, obtained by correlation with experiments, is typically in the range 9–11.⁹ The stability and N -factor results are obtained by a modified version of COSAL,^{1,2} wherein the stability equations are obtained by splitting the Navier–Stokes equation variables into mean flow and disturbance flow part:

$$U = \bar{U} + \hat{u}, \quad W = \bar{W} + \hat{w}, \quad V = \bar{V} + \hat{v}, \quad \text{etc.},$$

where the overbar denotes the mean flow and the hat denotes the disturbance quantity. Figure 6 defines streamwise (U) and spanwise (W) velocities in a three-dimensional boundary layer. The disturbance quantities are represented by the harmonic form:

$$\hat{u} = u e^{i(\alpha x + \beta z - \omega t)},$$

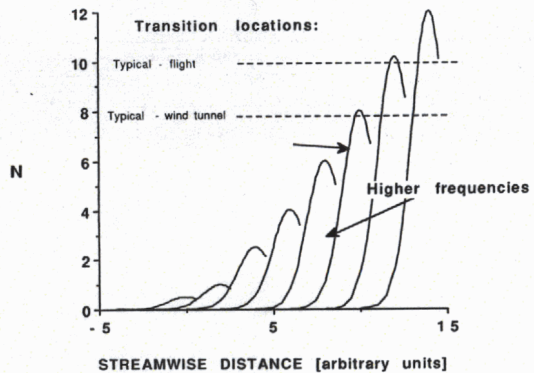


Fig. 7. Envelope method for amplification of constant frequency disturbances.

PEGASUS DELTA WING $T_w/T_{ad}=1$
COEFFICIENT OF PRESSURE

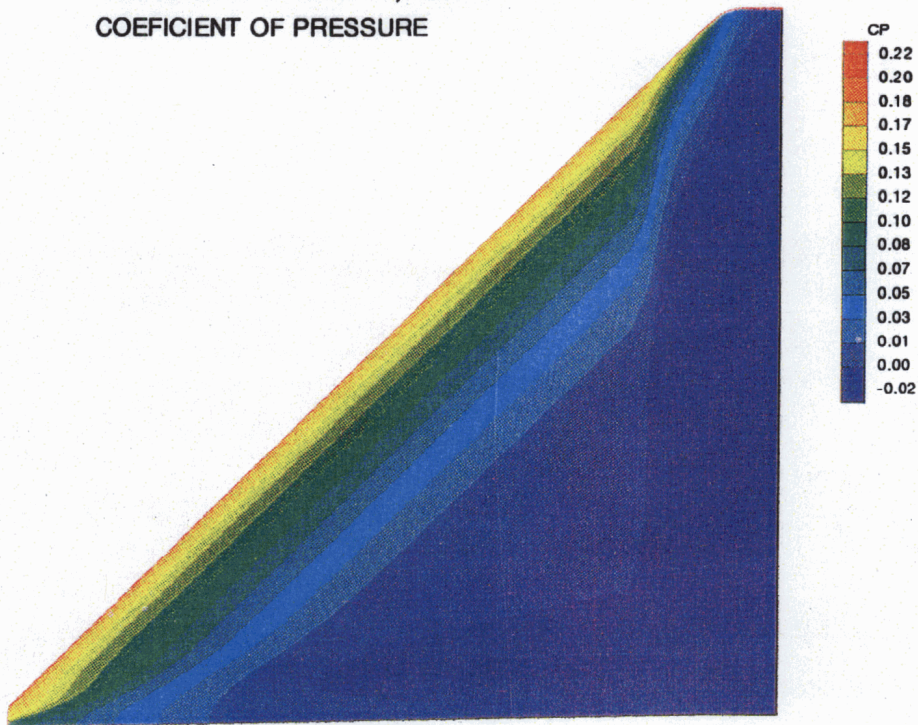


Fig. 8. Computed coefficient of pressure contours on the biconvex delta wing at Mach 6.

where α , β are streamwise and spanwise wavenumbers and ω is the frequency. The quasi-parallel flow assumption is made for the mean flow and the system of equations is linearized. An eigenvalue problem for α , β and ω is thus obtained, where the equations can be represented as:

$$\left(\mathbf{A} \frac{d^2}{dz^2} + \mathbf{B} \frac{d}{dz} + \mathbf{C} \right) \Phi = 0$$

where Φ is defined as a vector:

$$\Phi = [\alpha u + \beta v, w, p, T, \alpha v - \beta u].$$

The elements of the **A**, **B**, **C** matrices are given by Malik.¹

Temporal theory is used in COSAL, for which α and β are real and ω is complex. To compute the spatial growth rate σ from the temporal growth rate ω_i , the Gaster transformation¹⁰ is used:

$$\sigma = \left[\frac{\omega_i}{\text{Real}(V_g)} \right],$$

where V_g is the complex group velocity. The N -factor is calculated by integrating the spatial growth rate along a contour tangent to the group velocity on the surface:

$$N = \int \sigma ds,$$

where s is the contour from the neutral point (lower critical Reynolds number) to the transition front. The approach used here to define the growth rate is called the "envelope method", where the frequency is taken as real and the growth rate is maximized with respect to wavenumbers α and β . An illustration of the envelope method is shown in Fig. 7.

The linear stability modes present in a three-dimensional boundary layer at hypersonic speeds are:⁹ TS; crossflow; Gortler; and Mack's second mode. At high speed, the most amplified second mode is two-dimensional and the most amplified TS waves are oblique, with wave angle of 50–60°. The most amplified crossflow instability can have a wave angle of 70–90°. For swept wings, the transition phenomenon is often dominated by the crossflow instability associated with an inflectional crossflow velocity profile. Transition in a crossflow-dominated flow can be correlated with local crossflow Reynolds number,⁹ defined as:

$$Re_{cf} = \frac{W_{max} L_{0.01W_{max}}}{\nu},$$

where W_{max} is the maximum crossflow velocity and $L_{0.01W_{max}}$ is the distance from the wall to where the crossflow velocity is 1% of the maximum (also shown in Fig. 6). For subsonic flow, the crossflow Reynolds number at transition is of the order of 200. The transition crossflow Reynolds number increases with Mach number, as shown by the use of COSAL code.

PEGASUS DELTA WING $T_w/T_{ad}=1$
CROSS-FLOW REYNOLDS NUMBER

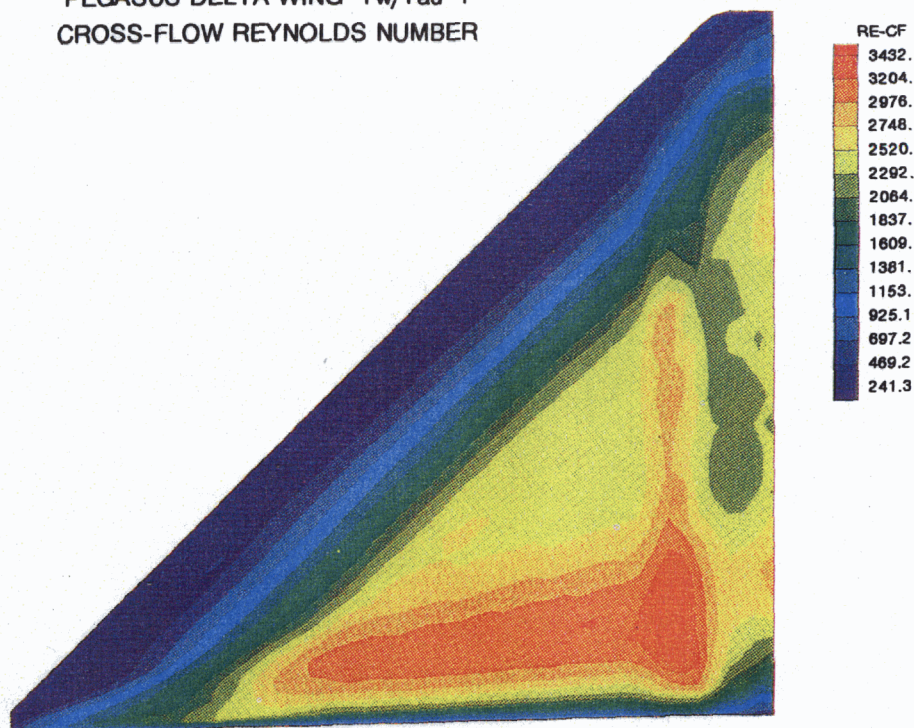


Fig. 9. Computed crossflow Reynolds number contours on the biconvex at Mach 6.

At high speed, transition can be correlated with a crossflow Reynolds number³ of:

$$Re_{t-cf} = 200 \left[1 + \frac{\gamma - 1}{2} M_c^2 \right],$$

where M_c is the local Mach number.

GLOVE SHAPE AND STABILITY RESULTS

In the glove design, it was essential to have laminar flow at the attachment line. It was also important to accentuate the crossflow instability by increasing the pressure gradient along the chord and by increasing the maximum thickness by 3.175 cm (1.25 in). It was important to ensure that the TS and the second mode instability are attenuated by having a favorable streamwise pressure over the entire glove. The wing glove is symmetrical and the chordwise shape is independent of spanwise location. Although the actual glove covers less than 30% of the wing surface, the design computations were made for a representative glove covering the entire wing surface.

Initially, computations were performed on several glove shapes, such as ellipse, super/sub-ellipse and biconvex configurations with an infinite swept-wing Euler and boundary-layer codes¹¹ along with the stability code COSAL. The results indicated that the crossflow Reynolds numbers and N -factors were highest on the biconvex glove. Hence, the final shape selected was biconvex, with the maximum thickness far back on the wing, blended in smoothly with the

nose to yield a smooth radius of curvature distribution along the chord.

These initial conical boundary-layer calculations are insufficient for precise description of the highly three-dimensional hypersonic flows because they ignore the viscous/inviscid interaction and the spanwise gradients. The fully three-dimensional Navier–Stokes code was therefore employed on the delta wing with this biconvex shape. The Navier–Stokes calculation of boundary-layer flow, for the degree of accuracy necessary for stability computations, requires a higher grid density, which might be limited due to memory and computer time considerations. Although real gas effect and shock waves can affect the boundary-layer stability at high speed, they are not accounted for in this study.

The computed pressure distribution on the surface of the biconvex wing is shown in Fig. 8. Figure 9 shows the computed crossflow Reynolds number contours for flight Mach 6 with the biconvex wing shape. In the current computations the local Mach number is 3.7–4.8, hence onset of transition should occur at Re_{t-cf} of 750–1100, based on the crossflow Reynolds number transition correlation described above.

Mean-flow interface code

Use of the Navier–Stokes solutions as an input for the COSAL code required an interface code,³ where the mean-flow solution is interpolated onto a surface-oriented boundary-layer grid, which is locally orthogonal with one coordinate defined normal to the

MACH NO = 6

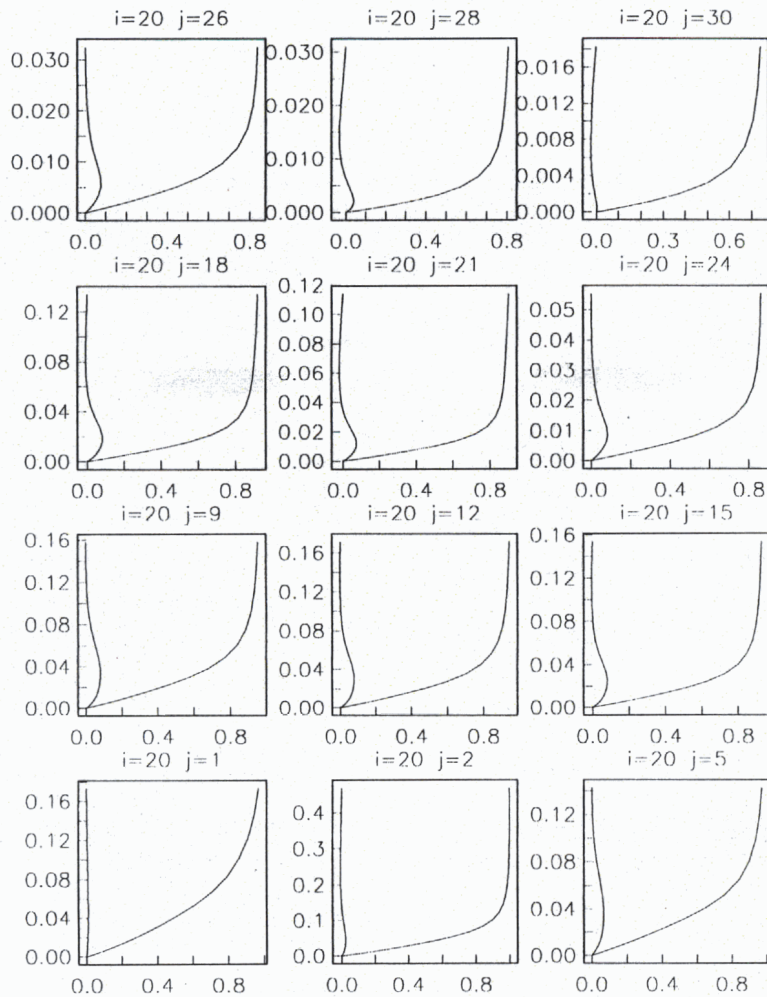


Fig. 10. Streamwise and crossflow velocity profiles at different spanwise location on the wing.

surface. The interpolation scheme used in the present study employed a linear-variation isoparametric quadrilateral element. Different criteria were used to determine the boundary-layer edge, such as absolute velocity gradient and total enthalpy. The streamwise and spanwise velocity at a given streamwise location and different spanwise locations are shown in Fig. 10.

Stability results

The COSAL code was used to investigate the stability characteristics and transition location of the biconvex wing mean flow. A wide range of frequencies was computed and the most amplified crossflow instability occurred at 3.5 kHz. Figure 11 shows the N -factor traces along the direction tangent to the group velocity for the most amplified frequency with growth rate maximized with respect to wavelength and wave angle along the integration path. The onset of transition is assumed to occur at $N = 9-10$. Wavelengths λ are of the order of 3-6 boundary-layer thicknesses δ and are shown in Fig. 12. The wave

angle ψ is defined with respect to the inviscid flow streamlines. The wave angles obtained from the stability calculations are shown in Fig. 13, and are in the range of $70-80^\circ$ with the angle decreasing as the calculation progresses in the direction tangent to the group velocity. The N -factor of 10 occurs at the end of the wing for a zero-frequency wave (stationary crossflow).

The parametric calculations indicate that the main factor that can be used to influence the transition is the altitude variation, since the crossflow Reynolds number is roughly proportional to the unit Reynolds number.

Attachment-line contamination

The success of the flight experiment will also depend upon whether or not the flow along the leading edge is laminar. Turbulence at the wing root can propagate along the leading-edge attachment line and cause the whole flow on the wing to become turbulent. This is referred to as "attachment-line

N-FACTOR
F=3500 Hz, MACH No.=6.

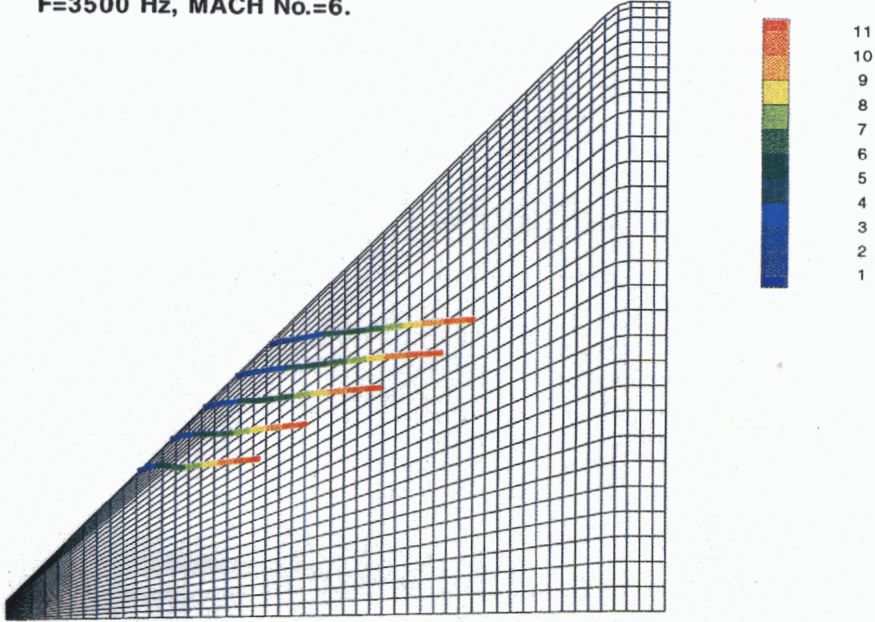


Fig. 11. *N*-Factor traces over the biconvex delta wing.

contamination". For the present experiment the implication was that the final glove shape be developed under the following constraints:

- (1) The attachment-line contamination and transition impose strict limits on the allowable leading-edge radius and two empirical criteria are utilized to determine the attachment-line boundary-layer state.
 (a) The Reynolds number based on the leading-edge

radius and free-stream conditions should be below 4×10^4 to avoid attachment-line contamination. This value is based on a cylindrical leading-edge shape and is a conservative estimate¹² (actual values are $5 \times 10^4 - 1 \times 10^5$). In Fig. 14 the state of the attachment-line boundary layer has been estimated using the Reynolds number based on leading-edge radius as a parameter. The figure indicates that 2.54 cm (1 in)

WAVE-LENGTH
F=3500 Hz, MACH No.=6.

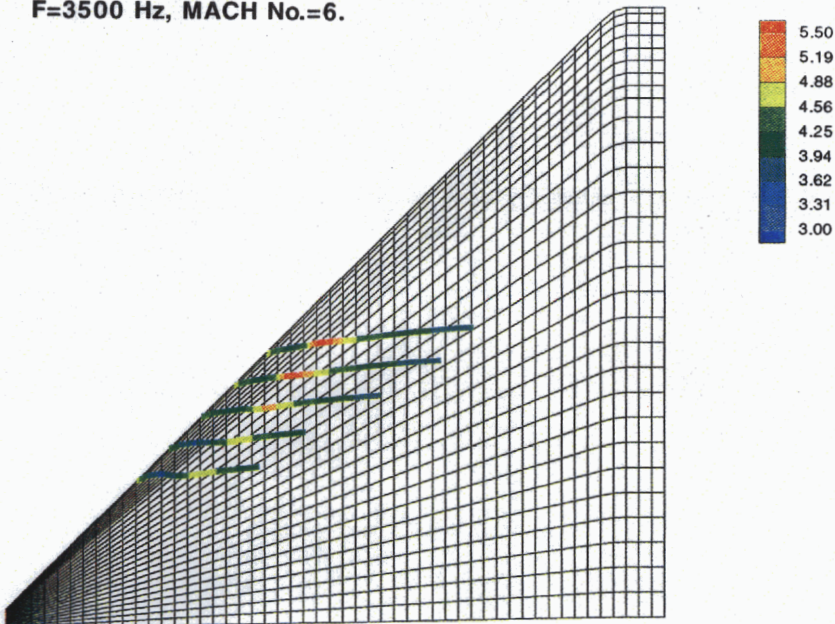


Fig. 12. Traces of wavelength normalized by boundary-layer thickness over the biconvex delta wing.

WAVE ANGLE

F=3500 Hz, MACH No.=6.

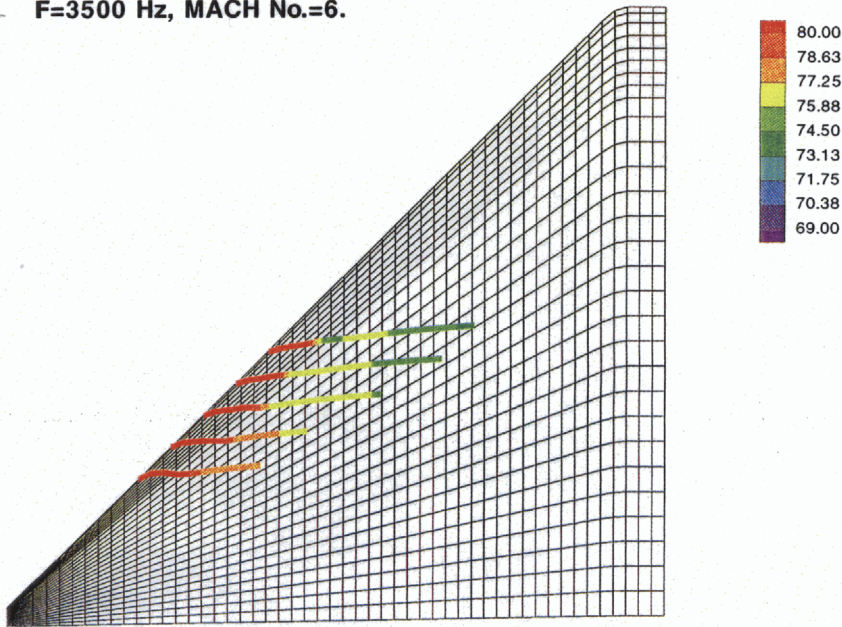


Fig. 13. Wave angle traces over the biconvex delta wing.

should be acceptable for most trajectories. (b) An attachment line similarity parameter by Poll¹² that takes into account the actual variation of the leading-edge radius is:

$$\bar{R}^* = \left\{ \frac{V_c^2 C_0}{v^* U_\infty U_1} \right\}^{1/2}$$

$$U_1 = \left[\frac{d(U_c/U_\infty)}{d(x/C_0)} \right]_{x=0}$$

which uses the local velocity components and the gradients at the attachment line to determine the probability of attachment-line transition. Here v^* is calculated at an intermediate temperature. The calculated value of \bar{R}^* for the described glove is about

170, where the necessary \bar{R}^* for the onset of transition is 245.

(2) The leading-edge radius of the existing Pegasus wing and the glove are 2.54 cm (1 in). The basic rule for the design is that the glove must be built up on the existing basic wing. Hence the glove had to be extended in front of the existing leading edge, causing a disturbance in the shock pattern around the leading edge of the wing. It was, therefore, essential to extend the fairing all the way to the wing-fuselage junction as shown in Fig. 15.

(3) The problem of ablation products flowing from the wing onto the glove must be addressed. The solution is to make the fairing from non-ablating material with a shape corresponding to the inviscid streamlines as shown in Fig. 15.

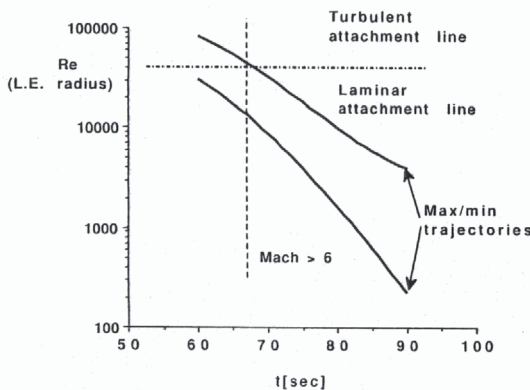


Fig. 14. Reynolds number based on 2.54 cm (1 in) leading-edge radius.

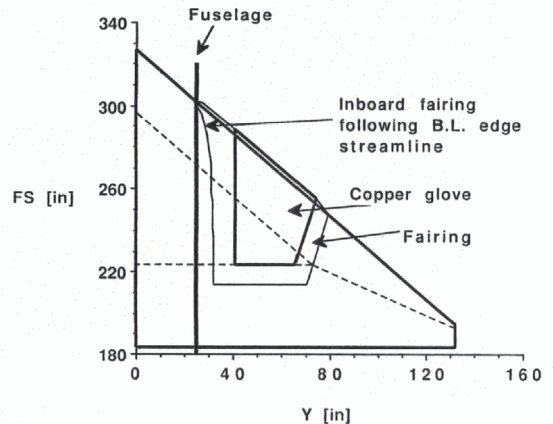


Fig. 15. Planform of glove and fairing on the basic wing.

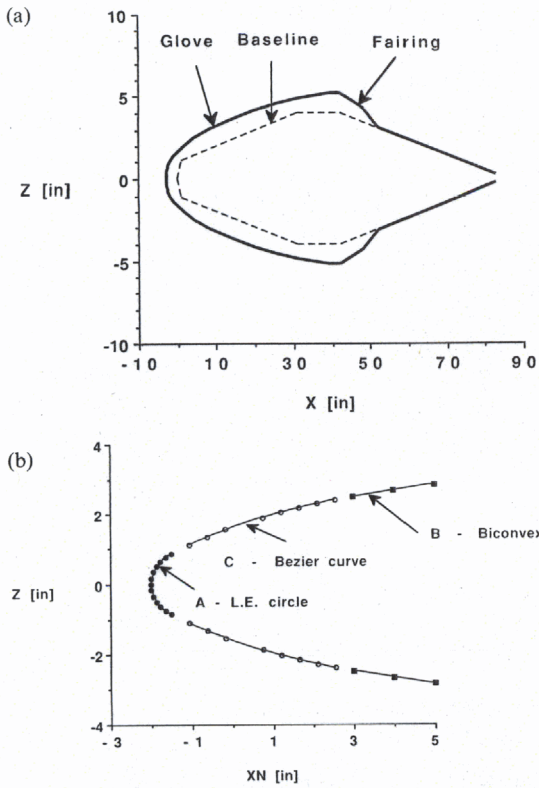


Fig. 16. (a) Basic wing and glove profiles along a chord line. (b) Glove shape in leading-edge region.

Three-dimensional glove definition

The glove section is shown in Fig. 16a and b. It consists of two circular arcs "A" and "B" as shown in Fig. 16b. These two circular arcs are connected by means of Bezier curve "C" fulfilling the continuity of ordinate, slope and curvature at the end points. The glove planform is shown in Fig. 15 and, in particular, the inboard fairing is critical. It was given a hyperbolic tangent shape in the spanwise direction and in the streamwise direction the shape corresponds to the inviscid streamlines.

COMPUTATIONS FOR THE FULL VEHICLE

The transition front could be affected by the shock waves generated from the fuselage-wing fairing, the glove-wing fairing, etc. To determine the location of these shocks, which may impinge on the glove surface, Navier-Stokes computations of the full baseline Pegasus vehicle were performed. The details of the computational methods and procedures used to examine the flow field for shocks or compression/expansion loci are described below.

Grid generation

The computational grid extends back only to the trailing edge of the delta wing, since the flight regime is hypersonic. The grid was generated by GRIDGEN,¹³ which consists of the three codes

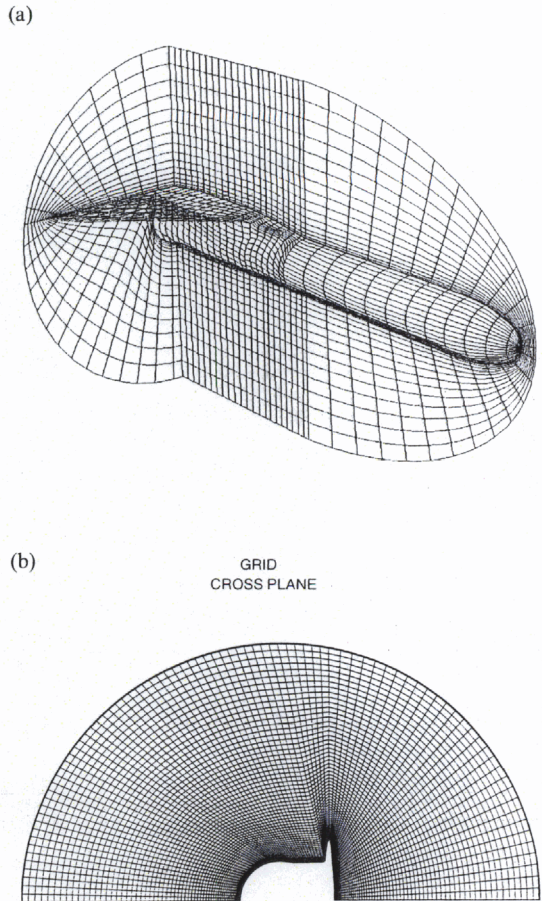


Fig. 17. (a) Pegasus grid on the surface, the symmetry plane and a downstream exit plane (20% of the grid shown). (b) Grid at a cross plane.

GRIDBLOCK, GRIDGEN2D, (both of which run on the IRIS workstation) and GRIDGEN3D (which runs on the CRAY computer). The code is a robust grid generation tool for multiple-block gridding over complex aircraft configurations. The GRIDBLOCK code provides an interactive graphics environment in which the multiple block structures and connectivity data are created and modified. Surface grids on these blocks are created interactively by GRIDGEN2D using algebraic and elliptic solvers. Similarly, the multi-block volume grid is generated by GRIDGEN3D with algebraic and elliptic solvers that take care of block interfaces. The grid generated around Pegasus had four blocks and a one-to-one correspondence of grid points at the interfaces. The outer boundary was elliptic in the front, with the bow shock generated by the blunt nose inside the computational domain. The grid points were clustered near the surface with 20-25 grid points in the boundary layer. The grid on the surface of vehicle, the symmetry plane and a downstream plane is shown in Fig. 17a and the grid at a streamwise location is shown in Fig. 17b. The total number of grid points used was close to 1,000,000.

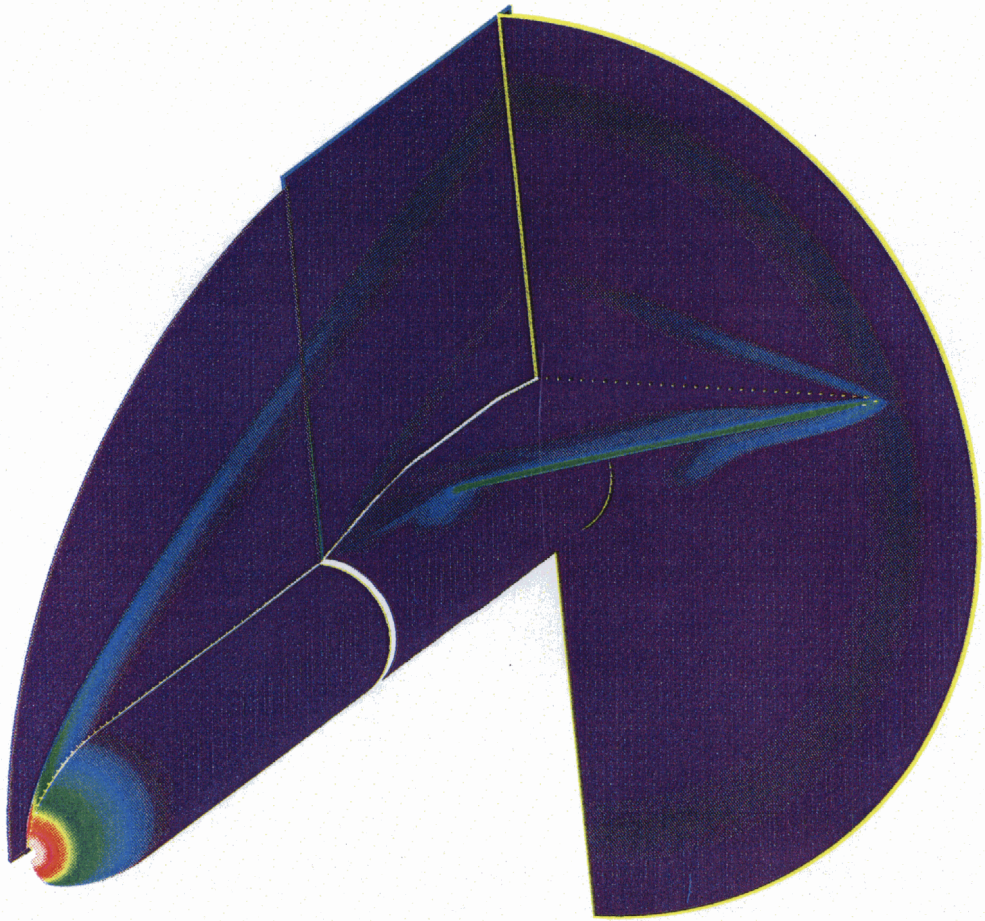


Fig. 18. Pressure contours at Mach 6 on the surface of the vehicle, the symmetry plane and a downstream plane.

Flow solver

The Navier–Stokes solver used was GASP⁷ (General Aerodynamic Simulation Program). It is a general-purpose flow solver developed by Walters

and associates. The code is capable of solving the Reynolds-averaged equations and subsets of the complete Navier–Stokes equations such as thin-layer Navier–Stokes equations, parabolized Navier–Stokes equations and Euler equations. The equations are

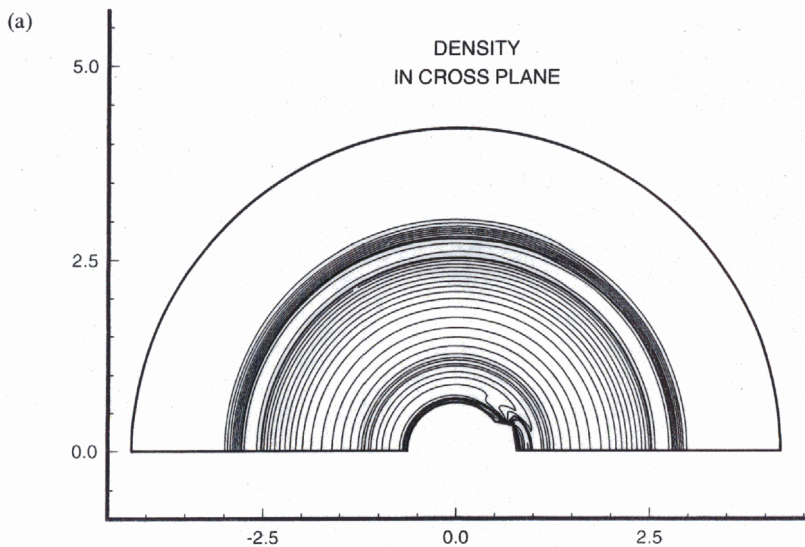


Fig. 19(a).

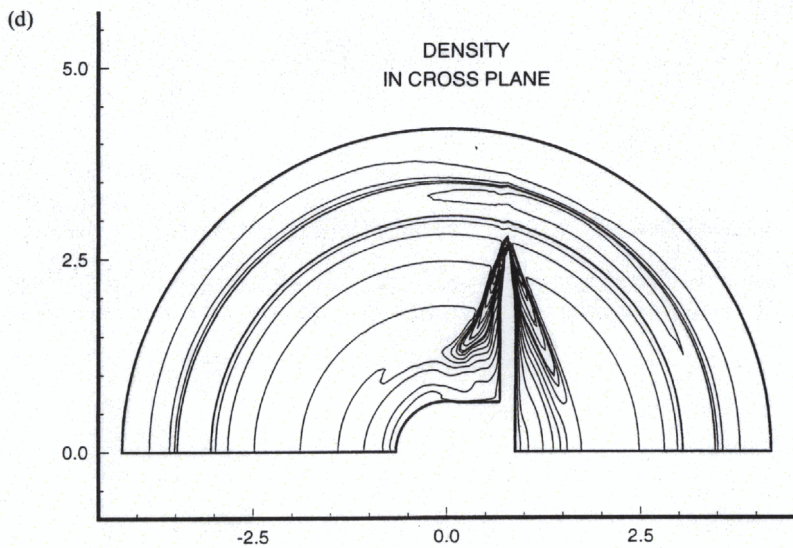
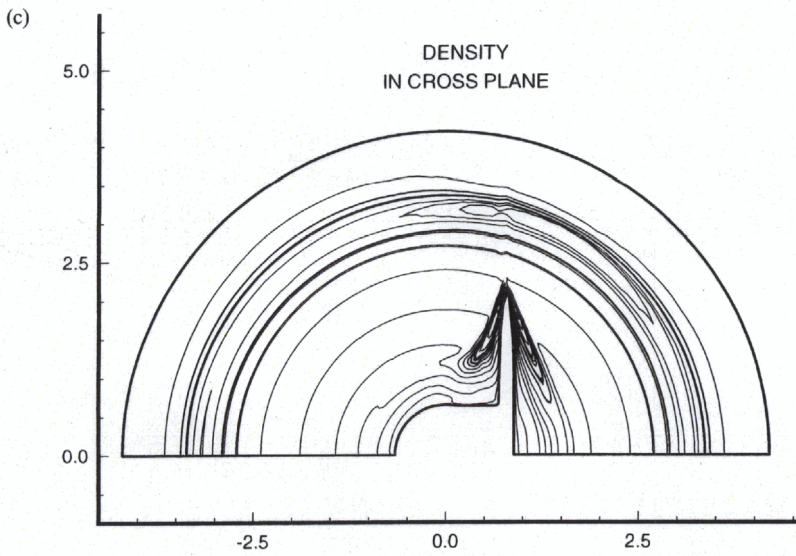
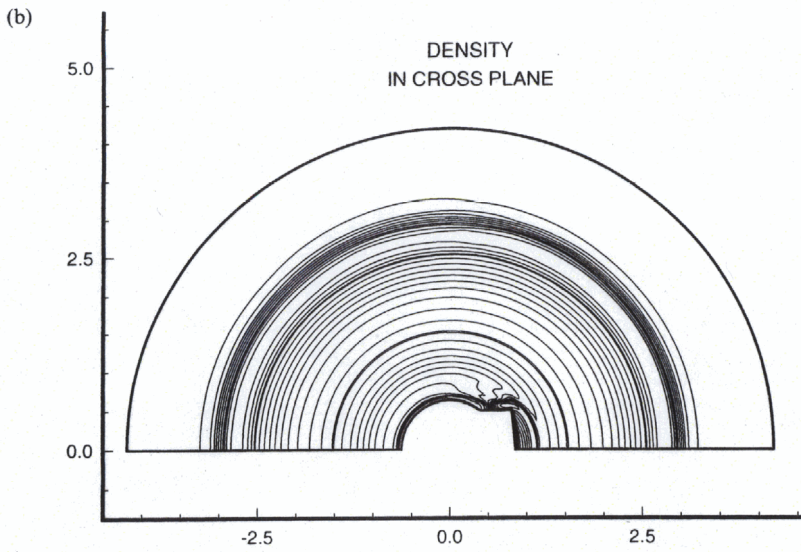


Fig. 19(b-d).
Fig. 19. The density contours on four cross planes.

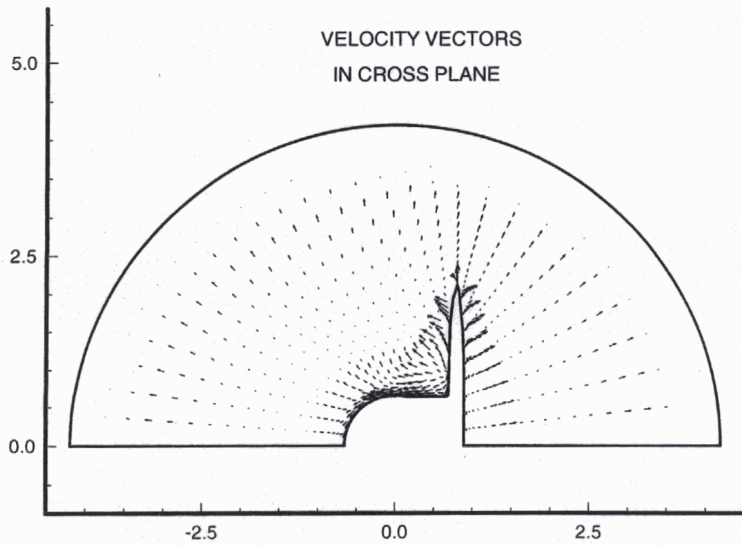


Fig. 20. Velocity vector plot for cross plane.

solved in a unified formulation for both time and space marching. The flow solver is based on a second/third-order upwind finite volume method and the fluxes are computed with a Riemann solver. It incorporates a general multi-block feature with one-to-one correspondence of grid points at the interface. Turbulence models and perfect and real gas capabilities are also included. A wide range of boundary conditions are accommodated.

Boundary conditions

At the solid surface of Pegasus, the no-slip condition was specified for velocity, and temperature ratio was specified for temperature boundary condition. The reflection of flow variables was employed at the plane of symmetry. At the far field, the free-stream values were specified and zeroth-order extrapolation of variables was used at the outflow boundary.

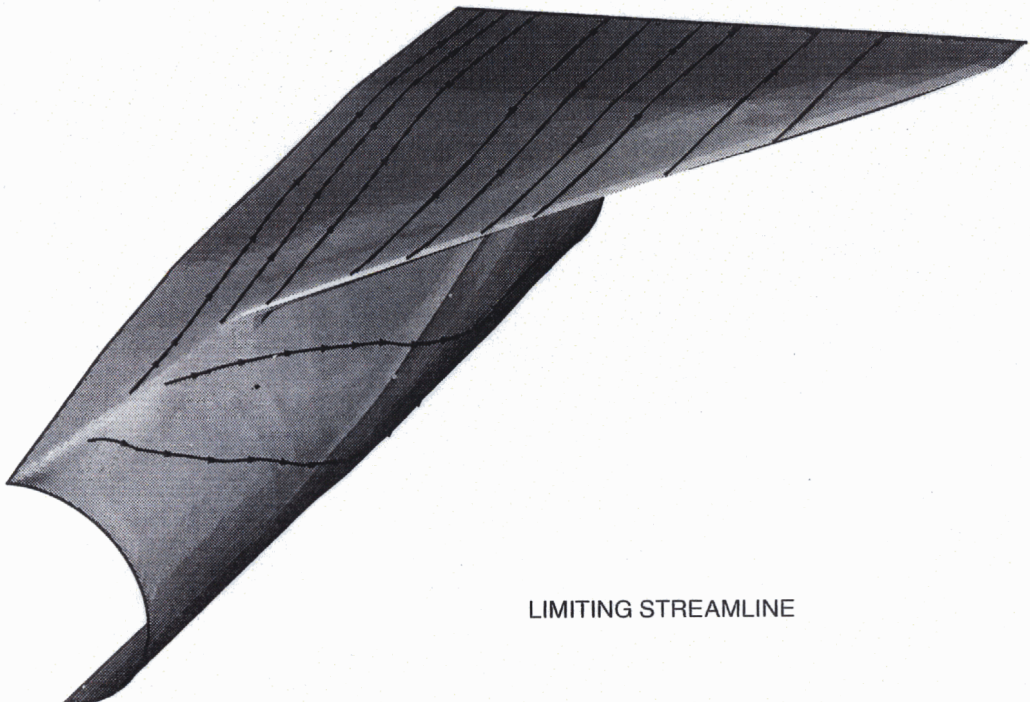


Fig. 21. The limiting streamline on the fairing and upper surface of the wing.

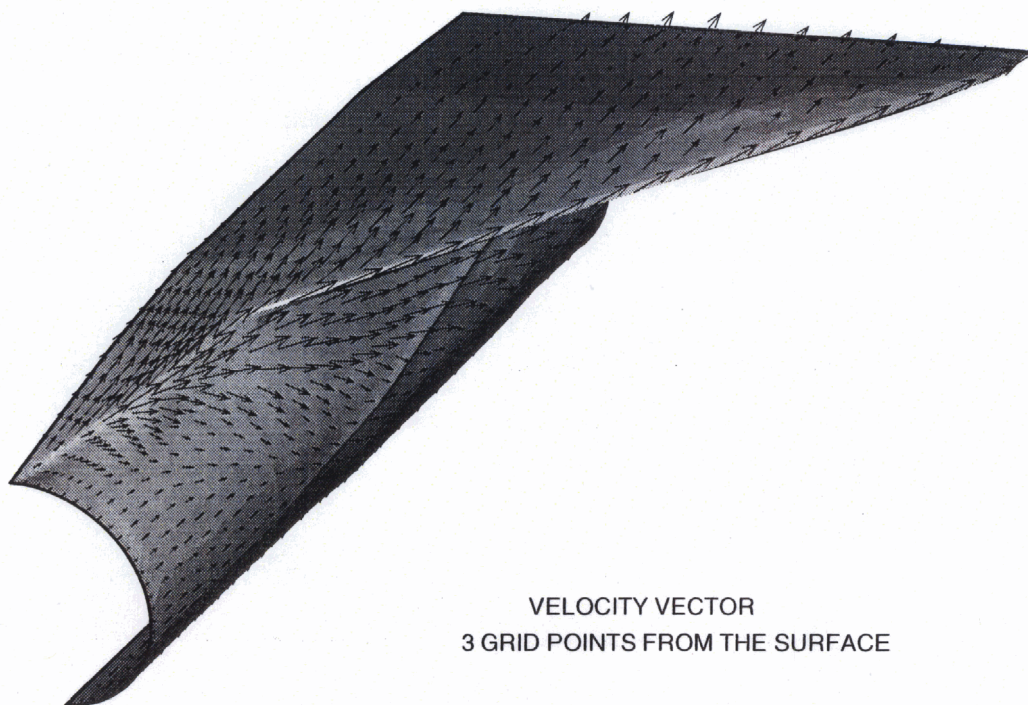


Fig. 22. Velocity vectors three grid points from the surface of the vehicle.

Results for the full vehicle

A three-dimensional Navier–Stokes computation was performed on the Pegasus vehicle for Mach 6, an altitude of 38 km and a corresponding Reynolds number of $9.0 \times 10^5 \text{ m}^{-1}$. The computations required approximately 9 h of CPU time on the CRAY-YMP at NASA Langley Research Center. Only the perfect gas case was considered in the present work. Figure 18 shows the pressure contours on the surface of the body, on the symmetry plane and on a downstream exit plane. The bow shock and the wing shock, which wrap around the delta wing, are clearly seen in the plot. The smoothness of the contours across the interfaces of different computational zones is also apparent. The density contours in the cross planes at four axial locations are shown in Fig. 19a–d. The plots in Fig. 19a and b show the shock generated from the fillet, whereas Fig. 19c and d show the wing shock and the bow shock. The shock generated at the fillet was of particular concern, since it might impinge on the wing at the glove location and hence affect the desired crossflow transition process. An examination of the solution indicates that, some distance downstream from the shock formation, the shape of the fillet causes an expansion that effectively cancels out the shock structure. A velocity vector plot for a cross plane at an axial location on the wing is shown in Fig. 20. Figures 21 and 22 show the limiting streamlines and velocity vectors close to the walls on the fairing and upper surface of the wing. The flow fields involved in the present experiment appear to be well-behaved from the transition point of view.

CONCLUSIONS AND CURRENT WORK

A wing glove has been designed for the Pegasus launch vehicle to give crossflow transition at 20–40% of the chord at Mach 6. For the present flight trajectory and for the selected glove leading-edge radius, the attachment-line Reynolds number is far below the critical Reynolds number necessary for the onset of transition along the attachment line. The Navier–Stokes computations show that the shocks generated at various junctions do not impinge on the glove.

Due to the large variation of Reynolds number with altitude, as well as the time-dependent heating of the glove, it is necessary to consider the chosen flight trajectory in detail to ensure the proper transition location. Care was taken in using the CFD codes for this transition study to adequately resolve the boundary layer. Although real gas effects and shock waves can affect the boundary-layer stability at hypersonic speed, they are not accounted for in this study.

Work is continuing to determine the effects of the finite glove span and to model the influences of the fairing on the glove flow. This will increase the complexity and size of the computational grid in the Navier–Stokes code. It is also necessary to go into more detail regarding the actual body geometry, since various geometrical anomalies associated with joints, antennas, handling plugs, etc., can trigger shocks which can influence the transition experiment. As wind tunnel data on the general flow properties of the Pegasus vehicle become available, comparisons will

be made for the baseline wing and the fully modeled part-span glove. While it is anticipated that transition data can be obtained and the designed glove shape will be retained from flight to flight, computations will be performed both as a guide in preparing for the next flight and to explore the agreement between the predicted flow characteristics and experimental flight data.

Acknowledgements—The authors are grateful to D. Bushnell, A. Kumar, M. R. Malik and C. L. Streett, NASA Langley Research Center, for many useful suggestions and encouragement. The work was performed under NASA contract NAS1-19299.

REFERENCES

1. M. R. Malik, "COSAL—a black-box compressible stability analysis code for transition prediction in three-dimensional boundary layers," NASA CR 165925, 1982.
2. R. Spall and M. R. Malik, "The linear stability of three-dimensional boundary layers over axisymmetric bodies at incidence," AIAA Paper No. 91-1640, June 1991.
3. V. Iyer and R. Spall, "Application of linear stability theory in laminar flow design," SAE 912116, Presented at the SAE Aerospace Technology Conference and Exposition, Long Beach, California, 23–26 August 1991.
4. M. R. Mendenhall, D. J. Lesieutre, S. C. Caruso, M. F. E. Dillenius and G. D. Kuhn, "Aerodynamic design of Pegasus[®]," AIAA Paper No. 91-0190, January 1991.
5. M. Mossier, G. Harris, B. Richards, D. Rovner and B. Carroll, "Pegasus[®] flight results," Presented at the 4th Annual AIAA/Utah State University Conference on Small Satellites, Lagan, Utah, 29 August 1990.
6. A. Kumar and R. A. Graves, Jr, "Numerical solution of the viscous hypersonic flow past a blunt cone at angle of attack," AIAA Paper No. 77-172, January 1977.
7. R. W. Walters, D. C. Slack, P. Cinnella, M. Applebaum and C. Frost, "A user's guide to GASP," Virginia Polytechnic Institute and State University, Blacksburg, Virginia, November 1990.
8. A. Moitra, "Euler solutions for high-speed flow about complex three-dimensional configurations," AIAA Paper No. 86-0246, January 1986.
9. M. R. Malik, "Stability theory for laminar flow control design," *Progress in Astronautics and Aeronautics* **123**, 3–46 (1990).
10. M. Gaster, "A note on the relation between temporally increasing and spatially increasing disturbances in hydrodynamic stability," *Journal of Fluid Mechanics* **14**, 222–224 (1962).
11. K. Kaups and T. Cebeci, "Compressible laminar boundary layer on swept and tapered wings," *Journal of Aircraft* **14**, 661–667 (1977).
12. D. I. Poll, "Transition description and prediction in three-dimensional flows," AGARD Report R-709, Paper 5, March 1984.
13. J. P. Steinbrenner, J. R. Chawner and C. L. Fouts, "The GRIDGEN 3D multiple block grid generation system," Vols I and II, WRDC-TR-90-3022, 1990.